Article

Fundamentals of lossless, reciprocal bianisotropic metasurface design

Luke Szymanski [1], Brian O. Raeker [1], Chun-Wen Lin[1] and Anthony Grbic [1,†*]

[1] Department of Electrical Engineering and Computer Science, University of Michigan; ljszym@umich.edu, braeker@umich.edu, chunwen@umich.edu, agrbic@umich.edu
* Correspondence: agrbic@umich.edu;
† Current address: 1301 Beal Avenue, EECS Building, Room 3238 Ann Arbor, Michigan 48109-2122

Abstract: Lossless, reciprocal bi-anisotropic metasurfaces have the ability to control the amplitude, phase, and polarization of electromagnetic wavefronts. However, producing the responses necessary to achieve this control with physically realizable surfaces is a challenging task. Here, several design approaches for bi-anisotropic metasurfaces are reviewed that produce physically realizable metasurfaces using cascaded impedance sheets. In practice, three or four impedance sheets are often used to realize bianisotropic responses which can result in narrow band designs that require the unit cells to be optimized to improve the performance of the metasurface. To address these issues in a systematic manner the notion of a metasurface quality factor is introduced for three-sheet metasurfaces. It is shown that the quality factor can be used to predict the bandwidth of a homogeneous metasurface, and can also be used to locate problematic unit cells when designing inhomogeneous metasurfaces. Several design examples are provided to demonstrate the utility of the quality factor including an impedance matching layer with maximal bandwidth and a gradient metasurface for plane wave refraction. In addition to these examples, several metasurfaces for polarization control are also reported including an isotropic polarization rotator and an asymmetric circular polarizer.

Keywords: Metasurfaces, bianisotropy, metasurface bandwidth

Citation: Szymanski, L.; Raeker, B.;Lin, C.W.; Grbic, A. Title. *Photonics* **2021**, *1*, 0. https://dx.doi.org/10.3390/photonics1010000

Received:
Accepted:
Published:

1. Introduction

Metasurfaces are the two-dimensional analogue of metamaterials, that interact with electromagnetic fields at a surface rather than throughout a volume [1]. They are often realized using electrically thin layers consisting of 2D arrays of subwavelength-spaced meta-atoms that can be homogenized. This allows for metasurfaces to be modelled using surface boundary conditions, called the generalized sheet transition conditions (GSTCs), which determine the interaction with an incident field through quasi-static surface polarizabilities, [2–4]. If the incident fields are time-varying, the surface polarizabilities produce equivalent electric and magnetic polarization currents. These equivalent currents can be related to surface admittances and impedances, [12,18,20,34–37]. The mechanisms by which electric and magnetic surface currents are induced on a metasurface determine its classification as an electric, magnetic, electric and magnetic, or bi-anisotropic metasurface. Purely electric metasurfaces contain only electric polarizabilites, which interact with only the electric field to produce electric currents. Purely magnetic metasurfaces contain only magnetic polarizabilities, which interact with only the magnetic field to produce magnetic currents. Electric and magnetic surfaces contain both electric and magnetic polarizabilities in a single sheet. Finally, a metasurface that is bianisotropic can contain electric and magnetic polarizabilities as well, as electro-magnetic and magneto-electric polarizabilities, i.e. magnetic polarization due to an electric field and electric polarization due to a magnetic field.

Bianisotropic metasurfaces provide the metasurface designer with the most degrees of freedom, making them useful for the extreme manipulation of electromagnetic fields. Bianisotropic metasurfaces include a wide range of both reciprocal and non-reciprocal responses. However, the focus here will be on design methods for reciprocal bianisotropic metasurfaces. Reciprocal bianisotropic metasurfaces can be split into two main classes: chiral and omega. Chiral metasurfaces contain meta-atoms that have broken mirror symmetry. This results in electric fields inducing magnetic currents along the impinging electric field, and magnetic fields inducing electric currents along the impinging magnetic field. These chiral responses alter the polarization state of the incident wave. On the other hand, omega metasurfaces contain meta-atoms with broken directional symmetry. This results in electric fields inducing magnetic currents orthogonal to the impinging electric field, and magnetic fields inducing electric currents orthogonal to the impinging magnetic field. This leads to an asymmetric scattering response from omega metasurfaces which maintains the polarization state.

Applications for chiral and omega bianisotropic metasurfaces fall into two main categories: those that guide and radiate electromagnetic waves and those that control reflection and transmission from a surface. Guided-wave bianisotropic metasurfaces shape fields along the surface through guided or leaky waves, and can be used to produce desired radiation patterns [5,6]. Whereas, metasurfaces that control reflection and transmission interact with incident wavefronts to manipulate the amplitude, phase, and polarization of the scattered fields. There are many design synthesis methods and realizations of planar and cylindrical bianisotropic metasurfaces that control reflection and transmission at frequencies ranging from microwave to optical using both composite (metal/dielectric) and all-dielectric metasurfaces [7–27]. This is by no means a complete representation of all the work in bianisotropic metasurfaces. For a more complete review of the literature see [28].

In this paper, the design and synthesis methods presented in [12] and [19] are reviewed and several design examples are provided. Additionally, a definition for the quality factor of a three-impedance-sheet metasurface is provided, that can be used to estimate the bandwidth of a homogeneous metasurface. This is demonstrated through the design of an impedance matching metasurface with maximal bandwidth. In addition to improving bandwidth, the quality factor can also aid designers in improving the performance of inhomogeneous metasurfaces. This is demonstrated by using the quality factor to guide the selection of appropriate unit cells in the design of a gradient metasurface for plane wave refraction.

2. Scattering from Bi-isotropic Metasurfaces

In this section, we describe the scattering performance of an omega-type bi-isotropic metasurface illuminated by a normally incident plane wave. The scattering analysis of bi-isotropic metasurfaces provided in this section follows that introduced in [12]. We consider a metasurface at a planar boundary between two regions of space, as shown in Figure 1, where the intrinsic wave impedance of region 1 is $\eta_1 = \sqrt{\mu_1/\epsilon_1}$ and of region 2 is $\eta_2 = \sqrt{\mu_2/\epsilon_2}$. The metasurface is at the $z = 0$ plane separating the two regions, and is illuminated by normally incident plane waves.

The interaction between the metasurface and an illuminating plane wave can be described via scattering parameters (S-parameters), which are the ratio between the scattered plane wave electric field and the incident plane wave electric field. The ratio of scattered electric field in region n to the incident electric field in region m for different polarizations is given as a 2×2 matrix.

$$\boldsymbol{S_{nm}} = \begin{pmatrix} S_{nm}^{xx} & S_{nm}^{xy} \\ S_{nm}^{yx} & S_{nm}^{yy} \end{pmatrix} \tag{1}$$

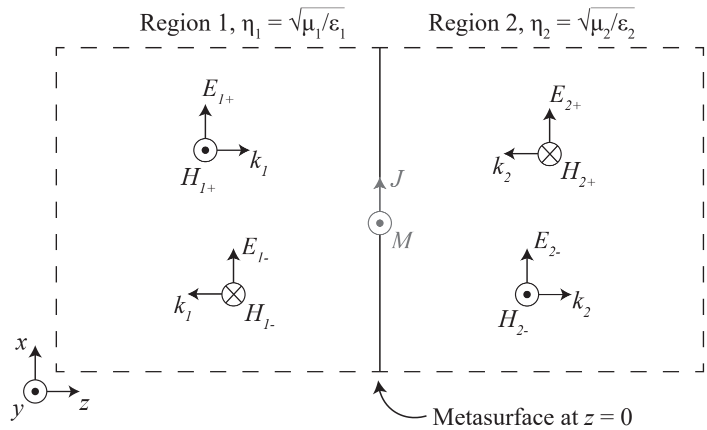

Figure 1. Geometry of a metasurface between two regions with different material properties. Equivalent surface current densities J (electric) and M (magnetic) describe the interaction of the metasurface with the tangential fields. Under illumination by a normally incident plane wave, each region can contain two plane waves denoted by $+$ for a wave propagating toward the surface or $-$ for a wave propagating away from the surface.

When viewed from region 1, $\boldsymbol{S_{11}}$ is the reflection coefficient and $\boldsymbol{S_{21}}$ is the transmission coefficient. Similarly, when viewed from region 2, the reflection coefficient is $\boldsymbol{S_{22}}$ and the transmission coefficient is $\boldsymbol{S_{12}}$.

In general, a bi-anisotropic metasurface can be modeled as a two-dimensional array of polarizable particles [4]. For time-varying illuminating fields, the polarizabilities can be effectively characterized using equivalent surface impedances [12,18,20,34–37]. The equivalent surface currents can then be related to the averaged, tangential electric and magnetic fields using surface parameters represented as 2×2 tensors: the electric sheet admittance tensor $\boldsymbol{Y}$, the magnetic sheet impedance tensor $\boldsymbol{Z}$, and the magneto-electric coupling tensors $\boldsymbol{\chi}$ and $\boldsymbol{\gamma}$. With these parameters, the electric and magnetic surface currents induced on the metasurface can be related to the average tangential fields and compared to the boundary conditions across the metasurface.

$$\begin{pmatrix} \boldsymbol{J} \\ M \end{pmatrix} = \begin{pmatrix} \boldsymbol{Y} & \boldsymbol{\chi} \\ \boldsymbol{\gamma} & \boldsymbol{Z} \end{pmatrix} \begin{pmatrix} \boldsymbol{E_{avg}} \\ \boldsymbol{H_{avg}} \end{pmatrix} = \begin{pmatrix} \hat{z} \times (\bar{\boldsymbol{H}}_{\boldsymbol{2}} - \bar{\boldsymbol{H}}_{\boldsymbol{1}}) \\ -\hat{z} \times (\bar{\boldsymbol{E}}_{\boldsymbol{2}} - \bar{\boldsymbol{E}}_{\boldsymbol{1}}) \end{pmatrix} \tag{2}$$

The variables $\boldsymbol{Y}$, $\boldsymbol{\chi}$, $\boldsymbol{\gamma}$, and $\boldsymbol{Z}$ relate the x- and y-polarized averaged field components to the x- and y-polarized current density components induced on the metasurface. The various electric field vectors are $\boldsymbol{E} = [E_x \quad E_y]^T$ and the magnetic field vector is $\boldsymbol{H} = [H_x \quad H_y]^T$ (surface current quantities $\boldsymbol{J}$ and $\boldsymbol{M}$ are similarly defined), where the averaged fields are $\boldsymbol{E_{avg}} = (\boldsymbol{E_1} + \boldsymbol{E_2})/2$ and $\boldsymbol{H_{avg}} = (\boldsymbol{H_1} + \boldsymbol{H_2})/2$. The electric admittance tensor is defined as

$$\boldsymbol{Y} = \begin{pmatrix} Y_{xx} & Y_{xy} \\ Y_{yx} & Y_{yy} \end{pmatrix} \tag{3}$$

with the other parameters similarly defined.

For a reciprocal metasurface, $\boldsymbol{Y} = \boldsymbol{Y}^T$, $\boldsymbol{\gamma} = -\boldsymbol{\chi}^T$, and $\boldsymbol{Z} = \boldsymbol{Z}^T$ [29]. Imposing isotropy on the surface parameters results in

$$\boldsymbol{Y} = Y\boldsymbol{I}, \qquad \boldsymbol{\chi} = -\chi\boldsymbol{n}, \qquad \boldsymbol{\gamma} = -\gamma\boldsymbol{n}, \qquad \boldsymbol{Z} = Z\boldsymbol{I} \tag{4}$$

where $\boldsymbol{I}$ is the 2×2 identity matrix and $\boldsymbol{n} = \begin{pmatrix} 0 & -1 \\ 1 & 0 \end{pmatrix}$.

Restricting the metasurface to omega-type bi-isotropy precludes polarization conversion by the metasurface. Therefore, the response for each polarization is identical. This allows us to analyze the metasurface as a two-port network for a single polarization, instead of as a four-port network when all polarizations were considered. The two-port S-parameters relate the electric field of the incident and reflected plane waves as

$$\boldsymbol{E}_{-} = \begin{pmatrix} E_{1-} \\ E_{2-} \end{pmatrix} = \begin{pmatrix} S_{11} & S_{12} \\ S_{21} & S_{22} \end{pmatrix} \begin{pmatrix} E_{1+} \\ E_{2+} \end{pmatrix} = \boldsymbol{S}\boldsymbol{E}_{+} \tag{5}$$

To calculate the S-parameters of the metasurface, consider an x-polarized plane wave as shown in Figure 1. Assuming the surface is isotropic, the boundary conditions of equation (2) simplify to

$$J_x = \frac{Y}{2}(E_{1x} + E_{2x}) + \frac{\chi}{2}(H_{1y} + H_{2y}) = -H_{2y} + H_{1y} \tag{6}$$

$$M_y = -\frac{\gamma}{2}(E_{1x} + E_{2x}) + \frac{Z}{2}(H_{1y} + H_{2y}) = -E_{2x} + E_{1x} \tag{7}$$

From equations (6) and (7), we obtain four equations by considering illumination from region 1 ($E_{2+} = 0$) and region 2 ($E_{1+} = 0$) separately. These four equations relate the S-parameters to the surface parameters of the metasurface. In each case, E_{1-} and E_{2-} are expressed in terms of the S-parameters and the illuminating electric field. Additionally, the assumption of plane wave illumination allows us to express the magnetic field quantities in terms of the electric field and wave impedance of each region. These four equations are simplified and assembled into a matrix equation to express the surface parameters in terms of S-parameters.

$$\frac{1}{2}\begin{pmatrix} Y & \chi \\ -\gamma & Z \end{pmatrix} = \begin{pmatrix} \frac{1}{\eta_1} - \frac{S_{11}}{\eta_1} - \frac{S_{21}}{\eta_2} & \frac{1}{\eta_2} - \frac{S_{22}}{\eta_2} - \frac{S_{12}}{\eta_1} \\ 1 + S_{11} - S_{21} & -1 - S_{22} + S_{12} \end{pmatrix} \begin{pmatrix} 1 + S_{11} + S_{21} & 1 + S_{22} + S_{12} \\ \frac{1}{\eta_1} - \frac{S_{11}}{\eta_1} + \frac{S_{21}}{\eta_2} & -\frac{1}{\eta_2} + \frac{S_{22}}{\eta_2} - \frac{S_{12}}{\eta_1} \end{pmatrix}^{-1} \tag{8}$$

The form of equation (8) is convenient for calculating surface parameters which will implement desired S-parameters. However, re-arranging equation (8) and simplifying to solve for the S-parameter quantities gives

$$S_{11} = \frac{1}{\sigma}\left(-Y + Z\frac{1}{\eta_1\eta_2} + \left[\frac{1}{4\eta_1}[(2-\gamma)(2-\chi) + YZ] - \frac{1}{4\eta_2}[(2+\gamma)(2+\chi) + YZ]\right]\right) \tag{9}$$

$$S_{12} = \frac{1}{\sigma}\left(\frac{1}{2\eta_2}[(2-\gamma)(2+\chi) - YZ]\right) \tag{10}$$

$$S_{21} = \frac{1}{\sigma}\left(\frac{1}{2\eta_1}[(2+\gamma)(2-\chi) - YZ]\right) \tag{11}$$

$$S_{22} = \frac{1}{\sigma}\left(-Y + Z\frac{1}{\eta_1\eta_2} - \left[\frac{1}{4\eta_1}[(2-\gamma)(2-\chi) + YZ] - \frac{1}{4\eta_2}[(2+\gamma)(2+\chi) + YZ]\right]\right) \tag{12}$$

$$\sigma = Y + Z\frac{1}{\eta_1\eta_2} + \left[\frac{1}{4\eta_1}[(2-\gamma)(2-\chi) + YZ] + \frac{1}{4\eta_2}[(2+\gamma)(2+\chi) + YZ]\right] \tag{13}$$

In the case of a lossless metasurface, the surface parameters $Y = jB$ and $Z = jX$ are purely imaginary while $\gamma = \chi = R$ are real quantities [29]. In this case, equations (9)-(12) can be further simplified as shown in equations (14)-(17). Note that $S_{21} = S_{12}$ only when $\eta_1 = \eta_2$, and $S_{11} = S_{22}$ only when $R = 0$ and $\eta_1 = \eta_2$.

$$S_{11} = \frac{1}{\sigma}\left(j\left[\frac{X}{\eta_1\eta_2} - B\right] + \left[\frac{1}{4\eta_1}\left[(2-R)^2 - BX\right] - \frac{1}{4\eta_2}\left[(2+R)^2 - BX\right]\right]\right) \tag{14}$$

$$S_{12} = \frac{1}{\sigma}\left(\frac{1}{2\eta_2}\left[4 - R^2 + BX\right]\right) \tag{15}$$

$$S_{21} = \frac{1}{\sigma}\left(\frac{1}{2\eta_1}\left[4 - R^2 + BX\right]\right) \tag{16}$$

$$S_{22} = \frac{1}{\sigma}\left(j\left[\frac{X}{\eta_1\eta_2} - B\right] - \left[\frac{1}{4\eta_1}\left[(2-R)^2 - BX\right] - \frac{1}{4\eta_2}\left[(2+R)^2 - BX\right]\right]\right) \tag{17}$$

$$\sigma = j\left[\frac{X}{\eta_1\eta_2} + B\right] + \left[\frac{1}{4\eta_1}\left[(2-R)^2 - BX\right] + \frac{1}{4\eta_2}\left[(2+R)^2 - BX\right]\right] \tag{18}$$

We can also determine the limitations placed on the S-parameters when passive, lossless, and reciprocal restrictions are enforced. For a bi-isotropic metasurface, the S-parameters represent a two-port network as described in equation (5). Each element is a complex number, so there are eight total variables (four real, and four imaginary quantities). For a reciprocal network, $S_{21} = S_{12}$ when the port impedances are the same. This relationship shows that both transmission coefficients are the same in amplitude and phase. However, a different relationship is needed for the case of the bi-isotropic metasurface since the port impedances are different. Reciprocity is satisfied when the transmission phase shift and transmitted power is the same for each direction of illumination. When the port impedances are not equal, the electric field amplitude will change depending on the wave impedance of the medium in order to satisfy reciprocity conditions, so $|S_{21}| \neq |S_{12}|$.

To determine the reciprocity relationship for a bi-isotropic metasurface, consider two cases: i) where the metasurface is illuminated from region 1 only and transmitted power is determined in region 2, and ii) the metasurface is illuminated from region 2 only and transmission measured in region 1. By equating the transmitted power in both cases, we arrive at

$$\frac{\eta_1}{\eta_2}|S_{21}|^2 = \frac{\eta_2}{\eta_1}|S_{12}|^2 \tag{19}$$

While equation (19) provides a relationship between the transmission coefficient magnitudes, reciprocity also requires that the transmission phase be the same. Applying this and assuming the wave impedance of each region is real, we arrive at

$$\sqrt{\frac{\eta_1}{\eta_2}}S_{21} = \sqrt{\frac{\eta_2}{\eta_1}}S_{12}. \tag{20}$$

Note that equations (15) and (16) satisfy this relationship since the metasurface parameters were restricted to be reciprocal.

To enforce the lossless condition, the time-average power absorbed by the metasurface must be zero. This is calculated as

$$P_{avg} = \frac{1}{2}\left\{\left(\begin{bmatrix}E_{1+}\\E_{2+}\end{bmatrix} + \begin{bmatrix}E_{1-}\\E_{2-}\end{bmatrix}\right)^T\left(\begin{bmatrix}H_{1+}\\H_{2+}\end{bmatrix} - \begin{bmatrix}H_{1-}\\H_{2-}\end{bmatrix}\right)^*\right\} = 0 \tag{21}$$

By applying the plane wave relation between the electric and magnetic fields, and expressing E_{1-} and E_{2-} in terms of the S-parameters from equation (5), equation (21) becomes

$$P_{avg} = \frac{1}{2}Re\left\{\left([E_+] + [S]\,[E_+]\right)^T\left([1/\eta]\,[E_+] - [1/\eta]\,[S]\,[E_+]\right)^*\right\} = 0 \tag{22}$$

where

$$[1/\eta] = \begin{bmatrix} 1/\eta_1 & 0 \\ 0 & 1/\eta_2 \end{bmatrix}, \qquad [E_+] = \begin{bmatrix} E_{1+} \\ E_{2+} \end{bmatrix}. \tag{23}$$

Simplifying equation (22) and utilizing the reciprocity relationship in (20) results in three equations which must be satisfied in order to implement a lossless and reciprocal metasurface.

$$1 = |S_{11}|^2 + \frac{\eta_1}{\eta_2}|S_{21}|^2 \tag{24}$$

$$1 = |S_{22}|^2 + \frac{\eta_1}{\eta_2}|S_{21}|^2 \tag{25}$$

$$0 = |S_{11}|\cos(\phi_{S11} - \phi_{S21} + \phi_{E1+} - \phi_{E2+}) + |S_{22}|\cos(\phi_{S21} - \phi_{S22} + \phi_{E1+} - \phi_{E2+}) \tag{26}$$

These three equations under-define the six independent scattering matrix variables. As a result, three variables can be chosen freely without violating the lossless and reciprocal conditions. Specifically, equations (24) and (25) provide the ability to choose one amplitude of the scattering matrix. If $|S_{21}|$ is chosen, as is commonly the case, then $|S_{11}| = |S_{22}|$, and a phase constraint is obtained from equation (26)

$$\phi_{S11} - \phi_{S21} = \phi_{S21} - \phi_{S22} + \pi \tag{27}$$

where two phase shifts of the S-parameters can be freely chosen.

Therefore, for a bi-isotropic metasurface to be both lossless and reciprocal, three degrees of freedom exist in its S-parameters: one S-parameter amplitude, and two S-parameter phases. These three degrees of freedom are set through design choices of the metasurface. Recall, that enforcing lossless and reciprocal behavior in the surface parameters for the bi-isotropic metasurface results in $Y = jB$, $Z = jX$, and $\gamma = \chi = R$. Thus, three distinct surface parameters can be chosen to achieve three desired scattering properties.

3. Bi-isotropic Metasurfaces: Bandwidth and Quality Factor

In practice, bi-isotropic metasurfaces typically rely on resonant structures to produce the strong field interactions required to perform desired field transformations. However, the use of resonances places inherent limitations on the bandwidth. In this section, the relationship between matching networks and bi-isotropic metasurfaces is considered, and the quality factor of a metasurface realized using three impedance sheets is defined. We demonstrate that the quality factor can be used as a metric to predict the metasurface bandwidth and identify unit cells that degrade the performance of inhomogeneous metasurfaces.

To understand the relationship between impedance matching networks and bi-isotropic metasurfaces, we consider the following example. Suppose there is a planar interface between air and alumina ($\varepsilon_r = 9.4$), as in Fig. 2, and the goal is to maximize the power transferred across the interface. Since the intrinsic wave impedances of the media are real, this amounts to minimizing the amplitude of the reflected wave. To do this, the input impedance of the metasurface must be equal to the wave impedance of the incident wave, Z_{in}. Since the two media have different wave impedances the metasurface must transform the wave impedance of the transmitted wave, Z_L, to that of the incident wave, Z_{in}. In this scenario, the metasurface acts as an impedance matching layer. Here, the impedance matching layer is analogous to an impedance matching network from circuit theory like an L or T-network, shown in Fig. 3. From circuit theory, it is known that a complex load impedance can be matched to complex source impedance using either an L-network, T- or π-network. The L-network contains two degrees of freedom allowing for the real and imaginary components of the input impedance to be matched. For an L-network, the solution is unique (all degrees of freedom are used) and no other

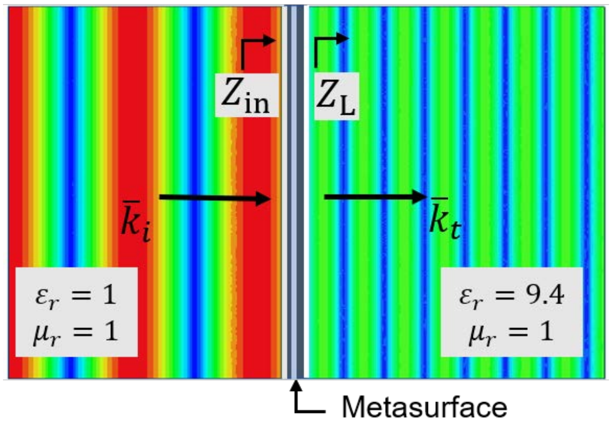

Figure 2. A metasurface at the interface between air and alumina half-spaces. The metasurface is used to impedance match a normally incident plane wave travelling from the region of air into the alumina.

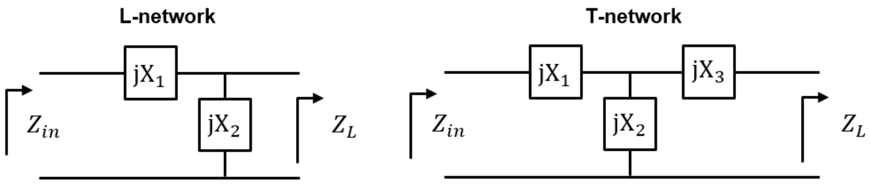

Figure 3. L and T circuit network topologies used for impedance matching in circuit theory.

characteristics of the impedance match, such as it's bandwidth or the transmission phase, can be controlled. Adding a third degree of freedom to the L-network produces a T- or π-network. This additional degree of freedom can be used to control the bandwidth or the transmission phase. Bi-isotropic metasurfaces are like T-matching networks for fields. They have three degrees of freedom that allow impedance matching with phase or bandwidth control [33]. To illustrate this idea, we consider a metasurface that impedance matches a normally incident plane wave on an air-alumina ($\varepsilon_r = 9.4$) interface over a maximum bandwidth, as shown in Fig. 2.

To design the impedance matching metasurface, recall that a bi-isotropic metasurface can be viewed as a two-port network that controls one scattering amplitude and two scattering phases. Therefore, designing a lossless, reflectionless, bi-isotropic metasurface is equivalent to designing a lossless two-port impedance matrix (Z-matrix) that impedance matches a load impedance $Z_L = |Z_L|e^{j\phi_L}$ to a source impedance $Z_i = |Z_{in}|e^{j\phi_{in}}$ with an arbitrary transmission phase ϕ_{21} [40]. To determine the Z-matrix that provides the desired functionality, consider a general lossless two-port Z-matrix,

$$\begin{pmatrix} V_1 \\ V_2 \end{pmatrix} = j\begin{pmatrix} X_{11} & X_{12} \\ X_{21} & X_{22} \end{pmatrix}\begin{pmatrix} I_1 \\ I_2 \end{pmatrix} \tag{28}$$

Imposing the impedance boundary conditions and enforcing power conservation on (28) produces the following system of equations,

$$\begin{pmatrix} 1 \\ r_v e^{j\phi_{21}} \end{pmatrix} = j\begin{pmatrix} X_{11} & X_{12} \\ X_{21} & X_{22} \end{pmatrix}\begin{pmatrix} 1 \\ -r_v e^{j\phi_{21}} \end{pmatrix} \tag{29}$$

where $r_v^2 = \frac{Z_L}{Z_{in}}\left|\frac{\cos\phi_{in}}{\cos\phi_L}\right|$ and $\phi_{21} = \angle V_2 - \angle V_1$. Splitting (29) into its real and imaginary components allows for the elements of the Z-matrix to be solved for in terms of Z_L, Z_{in} and ϕ_{21},

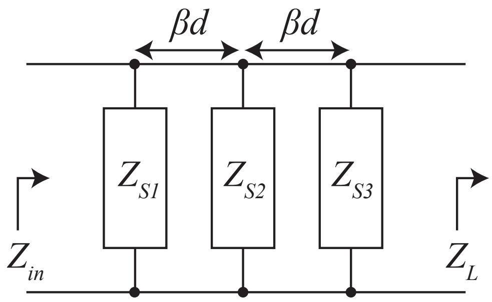

Figure 4. Bi-isotropic metasurface realized using three impedance sheets separated by dielectric spacers with thickness d.

$$\begin{pmatrix} X_{11} & X_{12} \\ X_{21} & X_{22} \end{pmatrix} = \begin{pmatrix} |Z_{in}|\cos(\phi_{21}-\phi_L) & |Z_{in}|r_v\cos(\phi_L) \\ |Z_{in}|r_v\cos(\phi_L) & |Z_L|\cos(\phi_{21}+\phi_{in}) \end{pmatrix} \csc(\phi_{21}+\phi_{in}-\phi_L) \tag{30}$$

From (30), it is clear that the required two-port network is reciprocal since $X_{12} = X_{21}$, and has three degrees of freedom. As in [12], three cascaded sheet impedances, shown in Fig. 4, can be used to realize a metasurface with a Z-matrix given by (30).

Expressing Fig. 4 in terms of it's Z-matrix, and solving for the necessary impedance sheets, results in the following expressions for the sheets in terms of the elements of (30),

$$Z_{s1} = -j\frac{Z_0\sin(\beta d)}{\cos(\beta d) + (\frac{X_{12}+X_{22}}{\det Z})Z_0\sin(\beta d)} \tag{31}$$

$$Z_{s2} = -j\frac{Z_0^2\sin^2(\beta d)X_{12}}{\det Z + X_{12}Z_0\sin(2\beta d)} \tag{32}$$

$$Z_{s3} = -j\frac{Z_0\sin(\beta d)}{\cos(\beta d) + (\frac{X_{12}+X_{11}}{\det Z})Z_0\sin(\beta d)}, \tag{33}$$

where $\det Z$ is the determinant of the Z-matrix and β and Z_0 are the wavenumber and wave impedance of the dielectric spacers, respectively. Once the input and load impedances, spacer thickness, and the transmission phase is specified, (30) can be used to determine the necessary impedance sheets to implement the metasurface.

To maximize the bandwidth of the impedance match, a method is needed for comparing the metasurface bandwidth for different transmission phases. Here, an expression of the metasurface quality factor as a function of the transmission phase is derived for this purpose. The quality factor of the three sheet metasurface is defined as,

$$Q = \omega_0\frac{2W_e}{P_d}, \tag{34}$$

where ω_0 is the angular resonant frequency, W_e is the average electric energy stored in the network at ω_0, and P_d is the power dissipated in the network. To calculate the quality factor using (34), the impedance sheets (31)-(33) are expressed in terms of lumped capacitances and inductances. The dielectric spacers in the metasurface are assumed to be electrically thin, so they can be modeled as lumped π-networks. Therefore, if the dielectric spacers are electrically thin and the source and load impedances are purely real, then the quality factor of the metasurface can be expressed as

$$Q = \frac{\omega_0}{2}\left(Z_{in}(C_{s1} + \frac{\beta d}{2\omega_0 Z_0}) + R_{int}(C_{s2} + \frac{\beta d}{\omega_0 Z_0}) + Z_L(C_{s3} + \frac{\beta d}{2\omega_0 Z_0})\right), \tag{35}$$

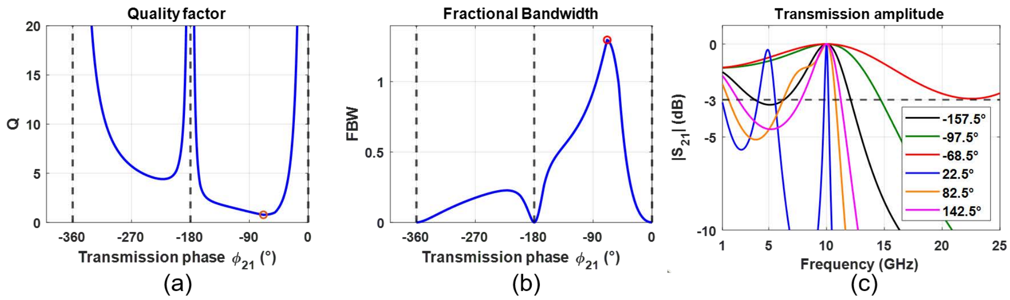

Figure 5. The quality factor, fractional bandwidth, and the magnitude of the frequency response for metasurfaces that provide impedance matching with six different transmission phases. (a) The quality factor is minimized when the transmission phase is $-68.5°$ (red circle). (b) The fractional bandwidth is maximized at $-68.5°$ (red circle). (c) Plots of the transmission amplitude over frequency for several transmission phases and the maximum bandwidth is observed when the transmission phase is $-68.5°$ as predicted by the quality factor.

where, $R_{int} = \frac{Z_{in}+Z_L+\sqrt{Z_{in}Z_L}\cos\phi_{21}}{\sin^2\phi_{21}} \frac{(Z_0 \sin\beta d)^2}{Z_{in}Z_L}$, and C_{si} is the capacitance of the ith impedance sheet (if the sheet is inductive then $C_{si} = 0$). If the load impedances are not purely real, the imaginary part of the load can be absorbed into either Z_{s1} or Z_{s3}, and (35) can still be used. The quality factor, Q, of the metasurface will be used to approximate the fractional bandwidth, $FBW = BW/f_0$, where BW is the 3 dB bandwidth of each unit cell. However, due to the presence of multiple resonances this approximation is only valid when the resonances are well separated in frequency.

The quality factor expression (35) can be used to maximize the bandwidth of an impedance matching bi-isotropic metasurface. For a normally incident plane wave, the relevant impedance is $Z_{in} = 377\Omega$. Let's assume that $Z_L = 123\Omega$, and the spacers are free-space with a thickness $d = \lambda_0/20$. Using (35) to calculate the quality factor and the fractional bandwidth versus transmission phase, produces Fig. 5. Fig 5 (b) shows that the maximum bandwidth occurs at a transmission phase of $\phi_{21} = -68.5°$. Fig 5 (a) plots (35) and predicts that this transmission phase maximizes the bandwidth, as shown in Fig. 5 (c). The metasurface with this transmission phase is composed of the following impedance sheets: $Z_{s1} = 1/(j\omega C_{s1}) = -j468.9\Omega$, $Z_{s2} = 1/(j\omega C_{s2}) = -j641.9\Omega$, and $Z_{s3} = j\omega L_{s3} = j38.5k\Omega$. The metasurface performance is simulated in Ansys HFSS using dispersive impedance sheets that correspond to the following lumped elements: $C_{s1} = 33.9fF$, $C_{s2} = 24.8fF$, and $L_{s3} = 612.7nH$. The transmission magnitudes from this simulation are shown in Fig. 6, where they are compared to a quarter-wave transformer and the bare interface without any impedance matching. The metasurface has a size and bandwidth comparable to a quarter-wave transformer. However, it doesn't require the realization of a medium with the dielectric constant $\varepsilon_r = \sqrt{9.4}$, which can be heavy and challenging to manufacture.

In practice, a metasurface's impedance sheets are typically realized using subwavelength metal or dielectric patterning on support structures. Here, we will consider the impact this has on the bandwidth of the metasurface. First, we will consider the effect of using subwavelength patterned sheets. Subwavelength unit cells that are non-resonant exhibit a response of either a capacitive or inductive sheet impedance [38,39]. This indicates that modeling the patterned sheets as impedance sheets should not result in a significant bandwidth reduction when the metasurface is realized in practice. However, if extreme impedance values that are difficult to realize are required it may be necessary to modify the design to include additional impedance sheets to avoid extreme impedance values. If impedance sheets cannot be realized at the design frequency due to manufacturing difficulties, an alternative design approach may be required, such as using detuned resonant elements. Their responses will be more narrowband.

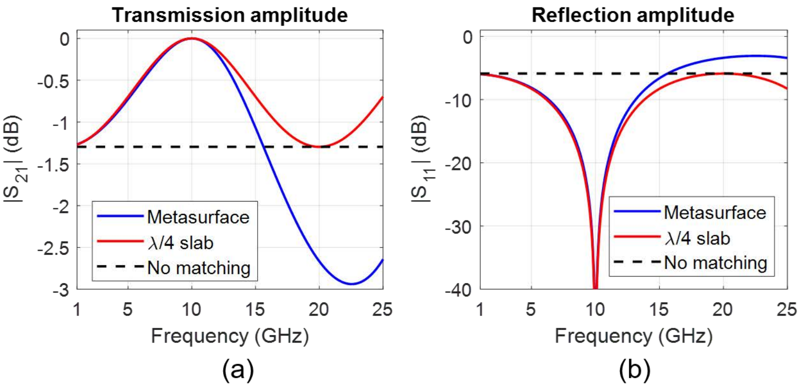

Figure 6. Plots of the transmission and reflection magnitudes for the interface with the metasurface ($\phi_{21} = -68.5°$), a quarter-wave transformer, and with no impedance matching (bare interface). The simulations of the metasurface were performed in Ansys HFSS. The metasurface has a bandwidth that is comparable to a quarter-wave transformer.

We will also consider the effect of using a dielectric spacer as the support structure. For a metasurface designed using a non-magnetic dielectric spacer with a relative permittivity ε_r its quality factor is given by,

$$Q = \frac{\omega_0}{2}\left(Z_{in}(C_{s1} + \frac{\varepsilon_r\varepsilon_0 d}{2}) + R_{int}(C_{s2} + \varepsilon_r\varepsilon_0 d) + Z_L(C_{s3} + \frac{\varepsilon_r\varepsilon_0 d}{2})\right). \tag{36}$$

If the dielectric spacer is electrically thin then the sheet capacitances can be approximated as,

$$C_{s1} = \frac{1}{\omega}(\frac{1}{\omega\mu d} + \frac{X_{22}+X_{12}}{\det(Z)}) - \frac{\varepsilon_r\varepsilon_0 d}{2} \tag{37}$$

$$C_{s2} = \frac{1}{\omega}(\frac{2}{\omega\mu d} + \frac{\det(Z)}{X_{12}}\frac{1}{(\omega\mu d)^2}) - \varepsilon_r\varepsilon_0 d \tag{38}$$

$$C_{s3} = \frac{1}{\omega}(\frac{1}{\omega\mu d} + \frac{X_{11}+X_{12}}{\det(Z)}) - \frac{\varepsilon_r\varepsilon_0 d}{2}, \tag{39}$$

when the sheet impedance Z_{si} is capacitive (see Appendix A). Otherwise, the impedance sheet is inductive and can be ignored in the calculation of the quality factor. Additionally, when the spacer is electrically thin R_{int} does not depend on the dielectric constant (see Appendix A). So the only terms in (36) that depend on the permittivity are the capacitance terms C_{si}, $\frac{\varepsilon_r\varepsilon_0 d}{2}$, and $\varepsilon_r\varepsilon_0 d$. Considering the terms $C_{s1} + \frac{\varepsilon_r\varepsilon_0 d}{2}$, $C_{s2} + \varepsilon_r\varepsilon_0 d$, and $C_{s3} + \frac{\varepsilon_r\varepsilon_0 d}{2}$ individually and using (37)-(39) in them, it becomes apparent that for capacitive impedance sheets the quality factor is unaffected by the dielectric spacer. However, if any of the impedance sheets are inductive then the dielectric spacer will increase the quality factor, thereby reducing the bandwidth of the metasurface.

In addition to bandwidth information, the quality factor also provides information that can guide the design of inhomogeneous metasurfaces where local periodicity is assumed. Obtaining good performance from a metasurface designed assuming local periodicity requires that neighboring unit cells produce fields that are approximately the same i.e. the fields vary smoothly along the surface without large discontinuities in amplitude or phase. In this work, it has been found that the quality factor and its first derivative with respect to transmission phase can help the designer select unit cells that satisfy the assumption of local periodicity.

The quality factor, given by (35), is divergent at transmission phases near $\phi_{21} = 0°, -180°$, and $-360°$, indicating that the unit cells required to achieve these transmission phases possess large quality factors. Large quality factors are associated with strong resonances which are sensitive to perturbations in the surrounding environment and are lossy when realized in practice. Therefore, these unit cells should be avoided. Additionally, areas where (35) is not smooth (i.e. points where the first derivative is discontinuous or undefined) indicate transmission phases where the reactance of at least one of the impedance sheets changes sign. These points should also be avoided because they identify transmission phases where the required reactance values display asymptotic behavior. This introduces rapid variations in the values of the impedance sheets and fields in the metasurface that invalidate the assumption of local periodicity.

To see how this information can be used, consider a metasurface embedded in free-space that refracts a normally incident plane wave to 70° at a frequency of $f_0 = 10GHz$. This requires a gradient metasurface: an inhomogeneous metasurface that imposes a linear phase gradient on an impinging wave-front to produce reflection or refraction into a desired direction [31]. Refraction requires the metasurface to alter the transverse wavenumber of an incident plane wave ($k_i = k\sin(\theta_i)$) to produce the desired refracted wavenumber ($k_t = k\sin(\theta_t)$), where k is the wavenumber in the surrounding medium. Therefore, the metasurface must impart transverse momentum equal to $\Delta k = k_t - k_i$. Practically, this is realized by discretizing the metasurface into N sub-wavelength unit cells of size $D = \frac{2\pi}{N\max(k_i,k_t)}$, each possessing a transmission phase ϕ_j such that $\Delta\phi = \phi_{j+1} - \phi_j = -\Delta k D$. Each unit cell must be reflectionless to maximize the transmitted power into the refracted wave. This means impedance matching and phase control are required, so (31)-(33) can be used to design the unit cells of the metasurface.

For this example, the metasurface will have 10 unit cells per transverse wavelength (in free-space) and the spacers will be assumed to be free-space with a thickness $d = \lambda_0/25$. As a first pass at the design, the metasurface is designed to impose a linear phase gradient with the unit cell transmission phases shown in Table 1. The required sheet impedances, shown in Fig. 7 (b), are solved for using (31)-(33) and one period (10 unit cells) of the metasurface is simulated in COMSOL using periodic boundary conditions. The results are shown in Fig. 7 (c).

The metasurface designed using this phase gradient exhibits significant reflections and the transmitted wave is not purely refracted. A slight perturbation of the linear phase gradient can be used to improve the performance. The appropriate perturbed phase gradient can found using the quality factor and its first derivative with respect to transmission phase. To find problematic transmission phases in the original design, plots of the quality factor and its first derivative are shown in Fig. 9. By inspecting the plots, four unit cells with problematic transmission phases are identified: 1, 5, 6, and 10. Unit cells 1, 5, and 6 are problematic because they are near points where (35) is not smooth, and unit cell 10 is problematic due to its large quality factor. To improve the performance of the metasurface, the problematic transmission phases are adjusted as shown in Table 1. These phase shifts reduce the maximum unit cell quality factor by approximately 10 and force the reactance of the impedance sheet's to change sign only once at $\phi_{21} = -180°$.

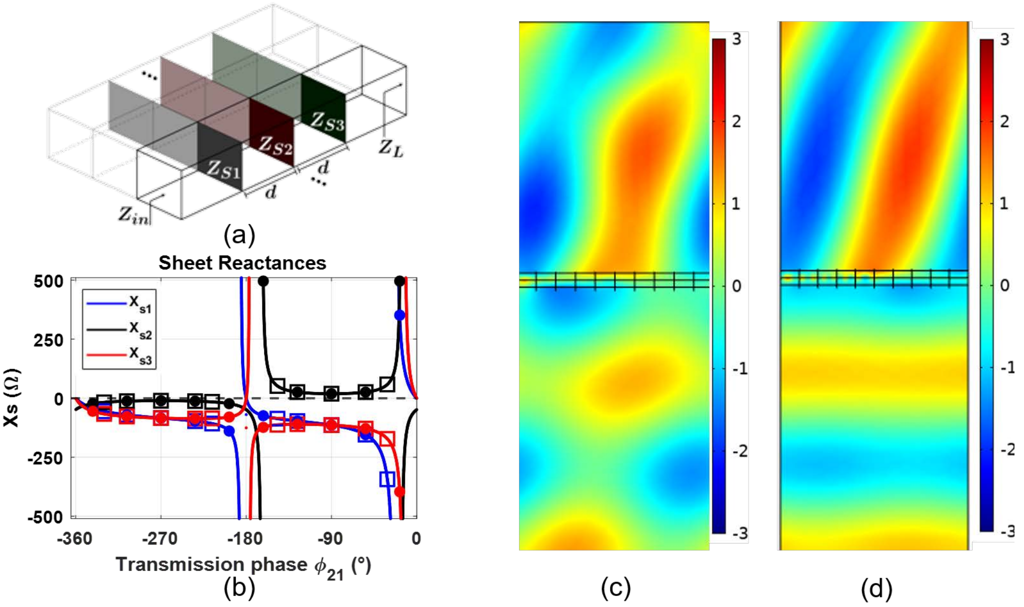

Figure 7. (a) Depiction of an inhomogeneous, bi-isotropic metasurface implemented as a three sheet cascade in free-space. (b) Plots of the sheet reactances for different transmission phases. The solid circles indicate the values used for the linear phase gradient and the empty squares indicate the sheet values used for the perturbed phase gradient. (c) Full-wave simulation results for the real part of the electric field using the metasurface with a linear phase gradient. (d) Full-wave simulation results for the real part of the electric field using the metasurface with a perturbed phase gradient.

Unit cell	ϕ_{21} (original)	ϕ_{21} (perturbed)
1	$-18°$	$-31°$
2	$-54°$	$-54°$
3	$-90°$	$-90°$
4	$-126°$	$-126°$
5	$-162°$	$-147°$
6	$-198°$	$-216°$
7	$-234°$	$-234°$
8	$-270°$	$-270°$
9	$-306°$	$-306°$
10	$-342°$	$-330°$

Table 1. Unit cell transmission phases (ϕ_{21}) used in the design of the gradient metasurface for plane wave refraction. The original phase gradient corresponds to the linear phase gradient. The perturbed phase gradient corresponds to the adjusted phases used to improve the performance of the metasurface.

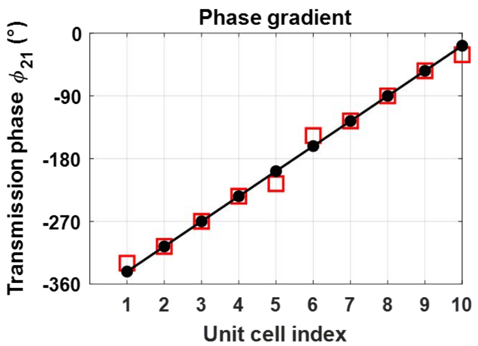

Figure 8. Comparison of the transmission phases used for the original and perturbed phase gradients. The solid black circles indicate the transmission phases used for the linear phase gradient. The empty red squares indicate the transmission phases used for the perturbed phase gradient

The metasurface is redesigned with the modified transmission phases and the required sheet impedances are shown in Fig. 7 (b). Ten unit cells of the metasurface are again simulated in COMSOL using periodic boundary conditions, and the results are shown in Fig. 7 (d). We see that the redesigned metasurface performs significantly better than the analytical design. This indicates that avoiding transmission phases which require a large quality factor or exist near non-smooth or asymptotic regions of $Q(\phi_{21})$ can improve the performance of gradient metasurfaces designed using the local periodicity assumption.

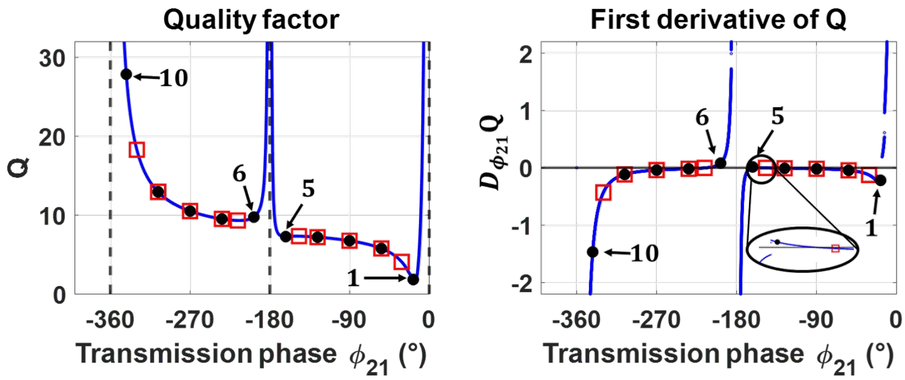

Figure 9. (a) The quality factor of the metasurface unit cells versus transmission phase. (b) The first derivative of the quality factor with respect to transmission phase. The solid black circles indicate values corresponding to the linear phase gradient and the hollow red squares indicate the adjusted values used for the perturbed phase gradient.

Violations of local periodicity (like those discussed above) can present challenges when realizing inhomogeneous metasurfaces where local periodicity has been assumed. Issues arising from these violations have been handled implicitly in the literature in a variety of ways. Such as in [20], where the phase gradient was altered to improve the metasurface's performance by reducing transmission losses. On the other hand, [40–42] made the sheet spacers extremely thin $d < \lambda/40$. This generally increases the quality factor of the unit cells but, it has the benefit of shifting the transmission phases where all three impedance sheets transition from capactive to inductive to occur at the same point. This means that shrinking the spacings makes it easier to select transmission phases that avoid regions where (35) is not smooth. As a result, extremely thin spacings can improve the design performance at the expense increasing manufacturing difficulties and producing higher quality factors: lower bandwidths. Alternatively, PEC [43] or PMC [26] baffles have been used to eliminate inter-cell coupling to validate the assumption of local periodicity. However, in practice the use of PEC baffles presents a manufacturing challenge and PMC baffles cannot be realized. These examples indicate a design trade-off between manufacturability and performance when realizing inhomogeneous metasurfaces. Using the quality factor as shown in this section provides an alternative way to improve design performance. It can be used to systematically identify problematic unit cells and adjust them where possible to allow for the trade-off between performance and manufacturability to be balanced. An alternative to this approach is to avoid the assumption of local periodicity and model interactions between unique unit cells using homogenization and integral equations as reported in, [44].

4. Scattering from Bi-anisotropic metasurfaces

While scattering of plane waves was analyzed for the simplified case of a bi-isotropic metasurface in Section 2, it is worthwhile to consider the general case where isotropy is not assumed. Following the general process of Section 2, the boundary conditions of equation (2) can be expressed in terms of the S-parameters (where each S-parameter term is the 2×2 matrix of equation (1)). Note that $\hat{z} \times \begin{bmatrix} E_x & E_y \end{bmatrix}^T = \boldsymbol{n}\begin{bmatrix} E_x & E_y \end{bmatrix}^T$. Expressing the surface parameters in terms of the S-parameters gives [12]

$$\frac{1}{2}\begin{pmatrix} \boldsymbol{Y} & \boldsymbol{\chi} \\ \boldsymbol{\gamma} & \boldsymbol{Z} \end{pmatrix} = \begin{pmatrix} \frac{\boldsymbol{I}}{\eta_1} - \frac{\boldsymbol{S_{11}}}{\eta_1} - \frac{\boldsymbol{S_{21}}}{\eta_2} & \frac{\boldsymbol{I}}{\eta_2} - \frac{\boldsymbol{S_{22}}}{\eta_2} - \frac{\boldsymbol{S_{12}}}{\eta_1} \\ \boldsymbol{n}(\boldsymbol{I} + \boldsymbol{S_{11}} - \boldsymbol{S_{21}}) & -\boldsymbol{n}(\boldsymbol{I} + \boldsymbol{S_{22}} - \boldsymbol{S_{12}}) \end{pmatrix} \begin{pmatrix} \boldsymbol{I} + \boldsymbol{S_{11}} + \boldsymbol{S_{21}} & \boldsymbol{I} + \boldsymbol{S_{22}} + \boldsymbol{S_{12}} \\ \boldsymbol{n}\left(\frac{\boldsymbol{I}}{\eta_1} - \frac{\boldsymbol{S_{11}}}{\eta_1} + \frac{\boldsymbol{S_{21}}}{\eta_2}\right) & -\boldsymbol{n}\left(\frac{\boldsymbol{I}}{\eta_2} - \frac{\boldsymbol{S_{22}}}{\eta_2} + \frac{\boldsymbol{S_{12}}}{\eta_1}\right) \end{pmatrix}^{-1} \tag{40}$$

Equation (40) can also be re-arranged so that the S-parameters are expressed in terms of surface parameters.

$$\begin{pmatrix} \boldsymbol{S_{11}} & \boldsymbol{S_{12}} \\ \boldsymbol{S_{21}} & \boldsymbol{S_{22}} \end{pmatrix} = \begin{pmatrix} \frac{\boldsymbol{I}}{\eta_1} + \frac{\boldsymbol{Y}}{2} - \frac{\boldsymbol{\chi n}}{2\eta_1} & \frac{\boldsymbol{I}}{\eta_2} + \frac{\boldsymbol{Y}}{2} + \frac{\boldsymbol{\chi n}}{2\eta_2} \\ -\boldsymbol{n} + \frac{\boldsymbol{\gamma}}{2} - \frac{\boldsymbol{Zn}}{2\eta_1} & \boldsymbol{n} + \frac{\boldsymbol{\gamma}}{2} + \frac{\boldsymbol{Zn}}{2\eta_2} \end{pmatrix}^{-1} \begin{pmatrix} \frac{\boldsymbol{I}}{\eta_1} - \frac{\boldsymbol{Y}}{2} - \frac{\boldsymbol{\chi n}}{2\eta_1} & \frac{\boldsymbol{I}}{\eta_2} - \frac{\boldsymbol{Y}}{2} + \frac{\boldsymbol{\chi n}}{2\eta_2} \\ \boldsymbol{n} - \frac{\boldsymbol{\gamma}}{2} - \frac{\boldsymbol{Zn}}{2\eta_1} & -\boldsymbol{n} - \frac{\boldsymbol{\gamma}}{2} + \frac{\boldsymbol{Zn}}{2\eta_2} \end{pmatrix} \tag{41}$$

As in the bi-isotropic case discussed in Section 2, analyzing the degrees of freedom helps determine the number of surface parameters required to realize a specificed S-matrix. In the bi-anisotropic case, both polarizations are taken into account, which leads to a 4×4 scattering matrix and 16 complex numbers as its entries. In most cases, reciprocity is desired for metasurfaces, resulting in a symmetric S-matrix (assuming the port impedances are identical)

$$\begin{pmatrix} \boldsymbol{S}_{11} & \boldsymbol{S}_{12} \\ \boldsymbol{S}_{21} & \boldsymbol{S}_{22} \end{pmatrix} = \begin{pmatrix} \boldsymbol{S}_{11} & \boldsymbol{S}_{12} \\ \boldsymbol{S}_{21} & \boldsymbol{S}_{22} \end{pmatrix}^T \tag{42}$$

which indicates that only 10 out of the 16 entries are actually independent. Since each complex number contains its real part and imaginary part, there are 20 free variables in total under the reciprocal condition. If we further require the metasurface to be lossless, the S-matrix also has to be unitary:

$$\begin{pmatrix} \boldsymbol{S}_{11} & \boldsymbol{S}_{12} \\ \boldsymbol{S}_{21} & \boldsymbol{S}_{22} \end{pmatrix}^T \begin{pmatrix} \boldsymbol{S}_{11} & \boldsymbol{S}_{12} \\ \boldsymbol{S}_{21} & \boldsymbol{S}_{22} \end{pmatrix}^* = \begin{pmatrix} 1 & 0 & 0 & 0 \\ 0 & 1 & 0 & 0 \\ 0 & 0 & 1 & 0 \\ 0 & 0 & 0 & 1 \end{pmatrix}. \tag{43}$$

By incorporating the reciprocal condition (42) into the lossless condition (43), one can expand (43) into 10 different equations, which impose 10 additional restrictions on the 20 free variables. Consequently, for a reciprocal and lossless bi-anisotropic metasurface, there are 10 degrees of freedom in total.

A similar conclusion can be drawn by considering the surface parameters. Recall that $\boldsymbol{Y} = \boldsymbol{Y}^T$, $\gamma = -\chi^T$, and $\boldsymbol{Z} = \boldsymbol{Z}^T$ for a reciprocal metasurface [29]. There are 3 free entries in both the $\boldsymbol{Y}$ and $\boldsymbol{Z}$ matrices, and 4 free entries in the γ or χ matrix. Moreover, for the metasurface to be lossless, $\boldsymbol{Y}$ and $\boldsymbol{Z}$ must have purely imaginary entries, while γ and χ must have purely real ones [29]. Again, it can be seen that the total degrees of freedom of the system is 10.

In practice, several sheets are usually cascaded and separated by dielectric spacers to form bi-anisotropic metasurfaces. Typically, these sheets only possess electric responses characterized by admittance tensors $\boldsymbol{Y}$, since they can be readily realized using metallic patterns. For bi-isotropic metasurfaces, or in the case where only a single polarization is of concern, we know that 3 sheets are enough to realize a specified response. However, the situation becomes more complicated for bi-anisotropic metasurfaces. When both polarizations are involved, a single lossless, reciprocal electric sheet provides three degrees of freedom under lossless and reciprocal conditions, i.e. the imaginary numbers Y_{xx}, Y_{yy} and $Y_{xy} = Y_{yy}$. Therefore, at most 4 sheets are required to realize an arbitrary reciprocal and lossless bi-anisotropic metasurface with 10 degrees of freedom. Although many bi-anisotropic metasurfaces can be realized with only 3 electric sheets, there are some cases in which introducing a fourth sheet is necessary. Examples include polarization rotators in [12], [19]. The fourth sheet not only provides the required degree of freedom but also enhances the operational bandwidth.

In order to synthesize a cascaded sheet design, a network analysis technique known as the wave matrix approach was adopted in [19]. Wave matrices relate the forward and backward propagating electric fields on one side of the scatterer to those on the other side. For an arbitrary scatterer shown in Fig. 10 (a), the wave matrix $\boldsymbol{M}$ is defined as:

$$\begin{pmatrix} \boldsymbol{E}_{\mathrm{L}}^{+} \\ \boldsymbol{E}_{\mathrm{L}}^{-} \end{pmatrix} = \boldsymbol{M} \begin{pmatrix} \boldsymbol{E}_{\mathrm{R}}^{+} \\ \boldsymbol{E}_{\mathrm{R}}^{-} \end{pmatrix}. \tag{44}$$

Similar to S-matrices, wave matrices contain information about the incident and reflected waves. The advantage of using wave matrices is that they significantly simplify the analysis of cascaded structures like ABCD matrices. The wave matrix of a cascaded structure can be obtained by simply multiplying the wave matrices of its constitutive

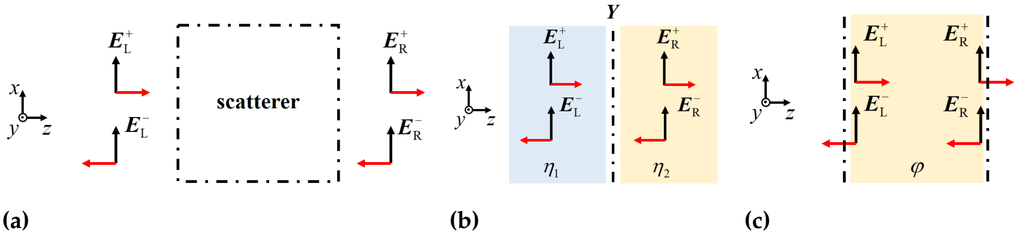

Figure 10. Illustration of the wave matrix and the constitutive blocks of the cascaded structure. (a) The definition of a wave matrix. (b) A metasurface interface between two dielectric media. (c) A dielectric spacer.

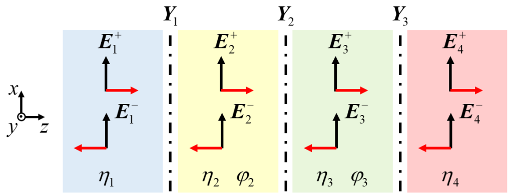

Figure 11. A cascaded metasurface structure consists of three sheets with only electric responses ($\gamma = \chi = \boldsymbol{Z} = \boldsymbol{0}$).

blocks. In our multi-layer metasurfaces, these blocks include metasurface interfaces across two dielectric media and dielectric spacers, as illustrated in Fig. 10 (b) and (c), respectively. Their corresponding wave matrices can be derived from boundary conditions and are explicitly shown in [19].

The procedure for synthesizing a reciprocal and lossless S-matrix is briefly outlined here. First, the desired S-matrix, $\boldsymbol{S}_{\text{spec}}$, is stipulated based on the required application. It is then converted to a wave matrix as follows [19]:

$$\boldsymbol{M}_{\text{spec}} = \begin{pmatrix} \boldsymbol{I} & \boldsymbol{0} \\ \boldsymbol{S}_{\boldsymbol{11},\text{spec}} & \boldsymbol{S}_{\boldsymbol{12},\text{spec}} \end{pmatrix} \begin{pmatrix} \boldsymbol{S}_{\boldsymbol{21},\text{spec}} & \boldsymbol{S}_{\boldsymbol{22},\text{spec}} \\ \boldsymbol{0} & \boldsymbol{I} \end{pmatrix}^{-1}, \tag{45}$$

where $\boldsymbol{0}$ represents a 2×2 null matrix. This wave matrix $\boldsymbol{M}_{\text{spec}}$ is known and set as the synthesis goal. It is worth noting that if $\boldsymbol{S}_{\boldsymbol{21},\text{spec}}$ has a zero determinant, taking the inverse matrix in (45) becomes invalid. In this case, a perturbation can be introduced into $\boldsymbol{S}_{\boldsymbol{21},\text{spec}}$ to alleviate this problem. For simplicity, it is assumed that this S-matrix can be realized by cascading 3 sheets. Accordingly, the targeted structure is displayed in Fig. 11 and the cascaded wave matrix that relates $\boldsymbol{E}_1^{\pm}$ to $\boldsymbol{E}_4^{\pm}$ is

$$\boldsymbol{M}_{\text{casc}} = \boldsymbol{M}^{(1)}_{\text{sheet}} \boldsymbol{M}^{(2)}_{\text{dielectric}} \boldsymbol{M}^{(2)}_{\text{sheet}} \boldsymbol{M}^{(3)}_{\text{dielectric}} \boldsymbol{M}^{(3)}_{\text{sheet}} \tag{46}$$

in which $\boldsymbol{M}^{(1)}_{\text{sheet}}$, $\boldsymbol{M}^{(2)}_{\text{sheet}}$ and $\boldsymbol{M}^{(3)}_{\text{sheet}}$ are the admittance tensors that need to be solved for. By setting $\boldsymbol{M}_{\text{spec}} = \boldsymbol{M}_{\text{casc}}$, and with some algebraic manipulation, one can find the admittance tensor of the second sheet $\boldsymbol{Y}_{\boldsymbol{2}}$ [19]:

$$\boldsymbol{e} \otimes \boldsymbol{Y}_{\boldsymbol{2}} = \frac{1}{A_2}\left((\boldsymbol{e} \otimes \boldsymbol{I})\boldsymbol{M}_{\text{spec}}(\boldsymbol{e} \otimes \boldsymbol{I}) - (\boldsymbol{e}\boldsymbol{t}_{\boldsymbol{1}}\boldsymbol{\Phi}_{\boldsymbol{2}}\boldsymbol{t}_{\boldsymbol{2}}\boldsymbol{\Phi}_{\boldsymbol{3}}\boldsymbol{t}_{\boldsymbol{3}}\boldsymbol{e}) \otimes \boldsymbol{I}\right). \tag{47}$$

The symbol $\otimes$ in (47) represents the Kronecker product of matrices and A_2 is some constant scalar. The matrix $\boldsymbol{t}_{\boldsymbol{1}}$ contains information about the dielectric interface where the first sheet is located, Φ_2 carries the phase information of the second dielectric spacer (t_2 , t_3 and Φ_3 are similarly defined), and $\boldsymbol{e}$ is a constant matrix [19]:

$$\boldsymbol{t}_{\boldsymbol{1}} = \frac{1}{2\eta_2}\begin{pmatrix} \eta_2 + \eta_1 & \eta_2 - \eta_1 \\ \eta_2 - \eta_1 & \eta_2 + \eta_1 \end{pmatrix}, \quad \boldsymbol{\Phi}_{\boldsymbol{2}} = \begin{pmatrix} e^{j\varphi_2} & 0 \\ 0 & e^{-j\varphi_2} \end{pmatrix}, \quad \boldsymbol{e} = \begin{pmatrix} 1 & 1 \\ -1 & -1 \end{pmatrix}. \tag{48}$$

Similarly, the admittance tensors of the first and third sheets $\boldsymbol{Y_1}$ and $\boldsymbol{Y_3}$ can be expressed in terms of $\boldsymbol{Y_2}$,

$$
\begin{aligned}
\boldsymbol{e} \otimes \boldsymbol{Y_1} &= \frac{1}{A_1}\Big[\boldsymbol{M}_{\mathrm{spec}}(\boldsymbol{e} \otimes \boldsymbol{I}) - (\boldsymbol{t_1 \Phi_2 t_2 \Phi_3 t_3 e}) \otimes \boldsymbol{I} - \frac{\eta_2}{2}(\boldsymbol{t_1 \Phi_2 e \Phi_3 t_3 e}) \otimes \boldsymbol{Y_2}\Big] \\
&\quad \cdot \Big(\boldsymbol{I} \otimes (\boldsymbol{I} + \frac{B_1}{A_1}\boldsymbol{Y_2})^{-1}\Big) \\
\boldsymbol{e} \otimes \boldsymbol{Y_3} &= \frac{1}{A_3}\Big(\boldsymbol{I} \otimes (\boldsymbol{I} + \frac{B_3}{A_3}\boldsymbol{Y_2})^{-1}\Big) \\
&\quad \cdot \Big[(\boldsymbol{e} \otimes \boldsymbol{I})\boldsymbol{M}_{\mathrm{spec}} - (\boldsymbol{e t_1 \Phi_2 t_2 \Phi_3 t_3}) \otimes \boldsymbol{I} - \frac{\eta_2}{2}(\boldsymbol{e t_1 \Phi_2 e \Phi_3 t_3}) \otimes \boldsymbol{Y_2}\Big]
\end{aligned}
\tag{49}
$$

where A_1, B_1, A_3 and B_3 are constants explicitly calculated in [19]. A more complicated synthesis procedure involving 4 cascaded sheets is also discussed in [19], but the main idea follows the 3 sheet case shown here.

5. Design Examples

In this section, several polarization-converting design examples are shown and discussed to illustrate the broad applicability of bi-anisotropic metasurfaces. For the details of the analysis and synthesis procedure please refer to [19]. All devices considered here are realized by cascading several electric sheets and thus can be realized in practice using subwavelength patterned surfaces. The admittances of the electric sheets can be characterized analytically [38,39,45], or through full-wave extraction methods. However, when the impedance sheets are cascaded to produce the bianisotropic unit cells, evanescent coupling resulting from the fine features of the patterning may shift the unit cell's response. To account for this, the impedance sheets will need to be designed such that the desired response of the unit cell is maintained. Several examples of metasurfaces demonstrating the feasibility of this approach at microwave and millimeter wave frequencies can be found in [11,12,20,46].

5.1. Asymmetric Circular Polarizer

The first device presented here is an asymmetric circular polarizer. The device converts a right-hand circularly polarized incident wave to a left-hand circularly polarized transmitted wave. On the contrary, when the incident wave is left-hand circularly polarized, it is totally reflected. An illustration of the operation is provided in Fig. 12 (a) [19]. Accordingly, the device has S-parameters:

$$
\boldsymbol{S}_{\boldsymbol{12},\mathrm{spec}} = \boldsymbol{S}^T_{\boldsymbol{21},\mathrm{spec}} = \frac{e^{j\phi}}{2}\begin{pmatrix} 1 & j \\ j & -1 \end{pmatrix}, \quad \boldsymbol{S}_{\boldsymbol{11},\mathrm{spec}} = \boldsymbol{S}_{\boldsymbol{22},\mathrm{spec}} = \frac{e^{j\phi}}{2}\begin{pmatrix} 1 & -j \\ -j & -1 \end{pmatrix}. \tag{50}
$$

for normal incidence.

Let us synthesize this asymmetric circular polarizer using the wave matrix approach [19]. This specified S-matrix leads to a $\boldsymbol{S}_{\boldsymbol{21},\mathrm{spec}}$ with a vanishing determinant. Hence, a perturbation is required in this case, as noted in the previous section:

$$
\boldsymbol{S}_{\boldsymbol{12},\mathrm{spec}} = \boldsymbol{S}^T_{\boldsymbol{21},\mathrm{spec}} = \frac{e^{j\phi}}{2}\begin{pmatrix} 1 & j \\ j & -e^{j1^\circ} \end{pmatrix}. \tag{51}
$$

This device can be realized by cascading three sheets. A unit cell of the device is shown in Fig. 12 (b). In this example, we stipulate both dielectric spacers to have a dielectric constant $\varepsilon_2 = \varepsilon_3 = 5$. It is assumed that the phase delay $\phi = 0$ and that the electrical lengths of both dielectric spacers are $\varphi_2 = \varphi_3 = 2\pi/5$. By substituting these parameters into the design equations, (47) and (49), the following sheet admittance tensors are obtained,

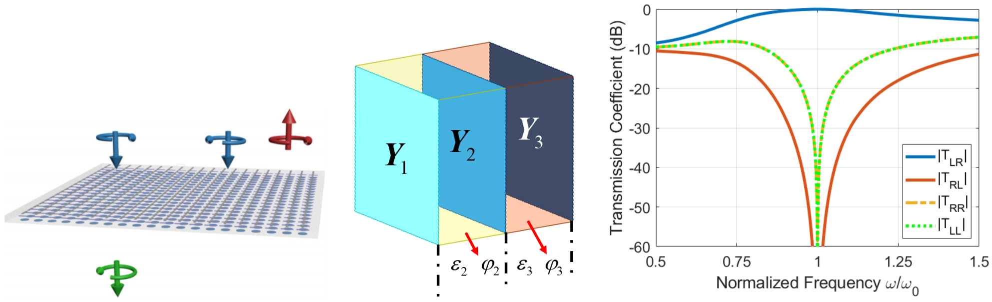

(a) **(b)** **(c)**

Figure 12. An asymmetric circular polarizer. (a) Polarization-converting operation of the metasurface [19]. (b) Unit cell of the asymmetric circular polarizer. (c) Simulated transmission coefficients.

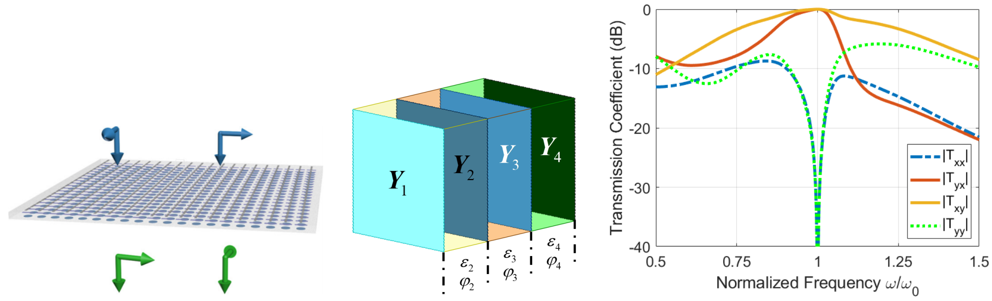

(a) **(b)** **(c)**

Figure 13. A linear polarization rotator. (a) Polarization-converting operation of the metasurface [19]. (b) Unit cell of the polarization rotator. (c) Simulated transmission coefficients.

$$\mathbf{Y_1} = \frac{j}{\eta_0}\begin{pmatrix} 0.73 & 1.00 \\ 1.00 & 0.72 \end{pmatrix}, \quad \mathbf{Y_2} = \frac{j}{\eta_0}\begin{pmatrix} 1268.31 & 5.52 \\ 5.52 & 1.43 \end{pmatrix}, \quad \mathbf{Y_3} = \mathbf{Y_1}. \tag{52}$$

For full-wave verification of the design, synthesized admittance values (52) are modeled in Ansys HFSS as anisotropic boundary conditions. At frequencies other than the design frequency, ω_0, the sheet admittances are assumed to obey Foster's reactance theorem. The eigenvalues of each sheet are first found by diagonalizing the tensors (52). If the resulting susceptances B_0 are positive, we assume a capacitive frequency dependence,

$$B_c(\omega) = \frac{\omega}{\omega_0} B_0, \quad \text{if} \quad B_0 > 0. \tag{53}$$

On the other hand, negative susceptances are assumed to possess an inductive response

$$B_l(\omega) = \frac{\omega_0}{\omega} B_0, \quad \text{if} \quad B_0 < 0. \tag{54}$$

The assumptions, (53) and (54), are in fact reasonable since the admittances are realized by simple metallic patterns. The simulated frequency response of the asymmetric circular polarizer is displayed in Fig. 12 (c), where the transmission characteristics match the specified performance at the operating frequency (51).

5.2. Polarization Rotator

The second device considered in this section is a reflectionless polarization rotator which rotates the polarization of any linearly polarized incident wave by 90°, as shown in Fig. 13 (a).

The stipulated S-parameters for this example are,

$$\mathbf{S}_{\mathbf{12},\mathrm{spec}} = \mathbf{S}^{T}_{\mathbf{21},\mathrm{spec}} = e^{j\phi}\begin{pmatrix} 0 & 1 \\ -1 & 0 \end{pmatrix}, \quad \mathbf{S}_{\mathbf{11},\mathrm{spec}} = \mathbf{S}_{\mathbf{22},\mathrm{spec}} = e^{j\phi}\begin{pmatrix} 0 & 0 \\ 0 & 0 \end{pmatrix}. \tag{55}$$

As discussed earlier, 4 sheets are required to reconstruct the stipulated S-matrix. With the unit cell shown in Fig. 13 (b), it is assumed that $\phi = \pi/4.5$, $\varepsilon_2 = \varepsilon_3 = \varepsilon_4 = 3.5$, and $\varphi_2 = \varphi_3 = \varphi_4 = \pi/5$. Following the synthesis procedure outlined in [19], the admittance tensors of each sheet are calculated to be:

$$\begin{aligned} \mathbf{Y_1} &= \frac{j}{\eta_0}\begin{pmatrix} 5.01 & 0.77 \\ 0.77 & 0.13 \end{pmatrix}, \quad \mathbf{Y_2} = \frac{j}{\eta_0}\begin{pmatrix} 9.30 & 0 \\ 0 & 1.00 \end{pmatrix} \\ \mathbf{Y_3} &= \frac{j}{\eta_0}\begin{pmatrix} 7.59 & -7.77 \\ -7.77 & 2.71 \end{pmatrix}, \quad \mathbf{Y_4} = \frac{j}{\eta_0}\begin{pmatrix} 2.57 & -1.30 \\ -1.30 & 2.57 \end{pmatrix}. \end{aligned} \tag{56}$$

The metasurface unit cell was simulated in Ansys HFSS, and the resulting frequency response is plotted in Fig. 13 (c). Again, the transmission characteristics match the specified performance at the design frequency.

6. Conclusions

In this paper, design procedures for realizing reciprocal bi-isotropic and bi-anisotropic metasurfaces using cascaded impedance sheets were reviewed. The design procedures use generalized sheet transition conditions (GSTCs) to relate bi-anisotropic surface parameters to the scattering parameters of the cascaded sheet impedances. Such approaches allow for metasurfaces with arbitrary lossless, reciprocal, bianisotropic responses to be realized in practice. These design methods were then used to realize several examples of practical devices with phase and polarization control. Specifically, they were used to realize an asymmetric circular polarizer and a reflectionless, polarization rotator.

In addition to these design procedures, the quality factor for metasurfaces composed of three impedance sheets was introduced. The quality factor was shown to predict the bandwidth of a homogeneous metasurface. This was demonstrated through the design of an impedance matching metasurface with maximal bandwidth. It was also shown that the quality factor could be used to improve the performance of inhomogeneous metasurfaces. This was demonstrated through the design of a gradient metasurface for plane wave refraction. The unit cell quality factor was used to identify cells that degraded the overall metasurface performance, and was used to select alternative unit cells that improved overall performance. Such an approach can be used to balance fabrication difficulty with performance for metasurface devices.

Author Contributions: Conceptualization, A.G.; methodology, L.S., C.W.L. and B.R.; software, L.S., C.W.L. and B.R.; validation, L.S., C.W.L. and B.R.; investigation, L.S., C.W.L. and B.R.; resources, A.G.; writing—original draft preparation, L.S., C.W.L. and B.R.; writing—review and editing, A.G., L.S., C.W.L and B.R.; visualization, L.S., C.W.L. and B.R.; supervision, A.G.; project administration, A.G.; funding acquisition, A.G. All authors have read and agreed to the published version of the manuscript.

Funding: This work was supported by the Office of Naval Research under Grant No. N00014-18-1-2536, the National Science Foundation under the Grant Opportunities for Academic Liaison with Industry (GOALI) program under Grant 1807940, the National Science Foundation Graduate Research Fellowship Program under Grant No. DGE 1256260, and the Chia-Lun Lo Fellowship at the University of Michigan.

Institutional Review Board Statement: Not applicable

Informed Consent Statement: Not applicable

Data Availability Statement: Not applicable

Conflicts of Interest: The authors declare no conflict of interest.

Appendix A

Here, the approximations used to calculate the quality factor of a metasurface with electrically thin spacers are derived. First, we will show that the internal matching resistance, R_{int}, is independent of the spacer's dielectric constant, ε_r. For an electrically thin spacer $\beta d << 1$. Using second-order small angle approximations, $\sin\beta d \approx \beta d$ and $\cos\beta d \approx 1 - \frac{(\beta d)^2}{2}$, in the expression for R_{int} yields,

$$R_{int} = \frac{Z_{in} + Z_L + \sqrt{Z_{in}Z_L}\cos\phi_{21}}{\sin^2\phi_{21}} \frac{(\omega\mu d)^2}{Z_{in}Z_L}, \tag{A1}$$

which does not depend on the dielectric constant of the spacer.

Next, we will derive the approximate expressions for the impedance sheets (31)-(33). Converting the $\sin(2\beta d)$ term in (32) to $2\sin(\beta d)\cos(\beta d)$ and making the same small argument approximations in (31)-(33),

$$Z_{s1} = -j\frac{\omega\mu d}{1 - \frac{\omega^2\mu\varepsilon_r\varepsilon_0 d^2}{2} + (\frac{X_{12}+X_{22}}{\det Z})\omega\mu d} \tag{A2}$$

$$Z_{s2} = -j\frac{(\omega\mu d)^2 X_{12}}{\det Z + 2X_{12}\omega\mu d(1 - \frac{\omega^2\mu\varepsilon_r\varepsilon_0 d^2}{2})} \tag{A3}$$

$$Z_{s3} = -j\frac{\omega\mu d}{1 - \frac{\omega^2\mu\varepsilon_r\varepsilon_0 d^2}{2} + (\frac{X_{12}+X_{11}}{\det Z})\omega\mu d}. \tag{A4}$$

Since we only need to consider capactive sheets in the calculation for the quality factor, we can set (A2)-(A4) equal to a capactive element $Z_{si} = 1/j\omega C_{si}$. Setting (A2)-(A4) equal to $1/j\omega C_{si}$, and solving for the sheet capacitances produces the following expressions,

$$C_{s1} = \frac{1}{\omega}(\frac{1}{\omega\mu d} + \frac{X_{22} + X_{12}}{\det(Z)}) - \frac{\varepsilon_r\varepsilon_0 d}{2} \tag{A5}$$

$$C_{s2} = \frac{1}{\omega}(\frac{2}{\omega\mu d} + \frac{\det(Z)}{X_{12}}\frac{1}{(\omega\mu d)^2}) - \varepsilon_r\varepsilon_0 d \tag{A6}$$

$$C_{s3} = \frac{1}{\omega}(\frac{1}{\omega\mu d} + \frac{X_{11} + X_{12}}{\det(Z)}) - \frac{\varepsilon_r\varepsilon_0 d}{2}. \tag{A7}$$

References

1. Holloway, C.L.; Kuester, E. F.; Gordon, J. A.; O'Hara, J.; Booth, J.; and Smith, D.R. An Overview of the Theory and Applications of Metasurfaces: Two-dimensional Equivalents of Metamaterials *IEEE Antennas Propag. Mag.* **2012**, *54*, 10–35.
2. Idemen, M. Straightforward derivation of Boundary Conditions on Sheet Simulating Anisotropic Thin Layer. *Electronics Lett.* **1988**, *24*, 663–665.
3. Idemen, M. Universal Boundary Relations of the Electromagnetic Field *J. Phys. Soc. Jpn* **1990**, *59*, 71–80.
4. Kuester, E. F.; Mohamed, M. A.; Piket-May, M.; Holloway, C. L. Averaged Transition Conditions for Electromagnetic Fields at a Metafilm *IEEE Trans. Antennas Propag.* **2003**, *51*, 2641–2651.
5. Tierney, B.B.; Grbic A. Controlling Leaky waves with 1-D cascaded metasurfaces *IEEE Trans. Antennas Propag.* **2018**, *66*, 2143–2146.
6. Abdo-Sánchez, E.; Chen, M.; Epstein, A.; Eleftheriades, G. V. A Leaky-Wave Antenna With Controlled Radiation Using a Bianisotropic Huygens' Metasurface *IEEE Trans. Antennas Propag.* **2019**, *67*, 108–120.
7. Kwon, D.H.;Werner, P.L.; and Werner, D.H. Optical planar chiral metamaterial designs for strong circular dichroism and polarization rotation *Opt. Express* **2008**, *16*, 11802–11807.
8. Kwon, D.H.; Werner, D.H.; Kildishev, A.V.; and Shalaev, V.M. Material parameter retrieval procedure for general bi-isotropic metamaterials and its application to optical chiral negative-index metamaterial design *Opt. Express* **2008**, *16*, 11822–11829.
9. Shaltout, A.;Shalaev, V.; Kildishev, A. Homogenization of bi-anisotropic metasurfaces *Opt. Express* **2013**, *21*, 21941–21950.
10. Niemi, T.; Karilainen, A. O.; Tretyakov, S. A. Synthesis of Polarization Transformers *IEEE Trans. Antennas Propag.* **2013**, *614*, 3102–3111.

11. Pfeiffer, C.; Zhang, C.; Ray, V.; Guo, L. Jay; Grbic, A. High Performance Bianisotropic Metasurfaces: Asymmetric Transmission of Light *Phys. Rev. Lett.* **2014**, *113*, 023902.
12. Pfeiffer, C.; Grbic, A. Bianisotropic Metasurfaces for Optimal Polarization Control: Analysis and Synthesis *Phys. Rev. Appl.* **2014**, *2*, 044011.
13. Wu, C.; Arju, N.; Kelp, G.; Fan, J.A.; Dominguez, J.; Gonzales, E.; Tutuc, E.; Brener, I.; and Shvets, G. Spectrally selective chiral silicon metasurfaces based on infrared Fano resonances. *Nat Commun* **2014**, *5*, 3892.
14. Tretyakov, S. A. Metasurfaces for general transformations of electromagnetic fields *Phil. Trans. R. Soc. A* **2015**, *373*, 20140362.
15. Achouri, K.; Salem, M. A.; Caloz, C. General Metasurface Synthesis Based on Susceptibility Tensors *IEEE Trans. Antennas Propag.* **2015**, *64*, 2977–2991.
16. Alaee, R.; Albooyeh, M.; Rahimzadegan, A.; Mirmoosa, M.S.; Kivshar, Y.S.; Rockstuhl, C. All-dielectric reciprocal bianisotropic nanoparticles *Phys. Rev. B* **2015**, *92*, 245130.
17. Odit, M.;Kapitanova, P.; Belov, P.; Alaee, R.; Rockstuhl, C.; Kivshar, Y.S.; Experimental realisation of all-dielectric bianisotropic metasurfaces *Appl. Phys. Lett.* **2016**, *108*, 221903.
18. Epstein, A.; Eleftheriades, G. V. Arbitrary Power-Conserving Field Transformations With Passive Lossless Omega-Type Bianisotropic Metasurfaces *IEEE Trans. Antennas Propag.* **2016**, *64*, 3880–3895.
19. Ranjbar, A.; Grbic, A. Analysis and synthesis of cascaded metasurfaces using wave matrices *Phys. Rev. B* **2017**, *95*, 205114-1–12.
20. Chen, M.; Abdo-Sánchez, E.; Epstein, A.; Eleftheriades, G. V. Theory, design, and experimental verification of a reflectionless bianisotropic Huygens' metasurface for wide-angle refraction *Phys. Rev. B* **2018**, *97*, 125433.
21. Kwon, D.H.; Ptitcyn, G.; Díaz-Rubio, A.; Tretyakov S.A. Transmission Magnitude and Phase Control for Polarization-Preserving Reflectionless Metasurfaces *Phys. Rev. Appl.* **2018**, *9*, 034005.
22. Ranjbar, A.; Grbic, A. Broadband, Multiband, and Multifunctional All-Dielectric Metasurfaces *Phys. Rev. Appl.* **2019**, *11*, 054066.
23. Sipus, Z.; Bosiljevac, M.; and Grbic, A. Modelling cascaded cylindrical metasurfaces using sheet impedances and a transmission matrix formulation *IET Microw. Antennas Propag.* **2018**, *12*, 1041–1047.
24. Sipus, Z.; Eres, Z.; and Barbaric, D. Modeling Cascaded Cylindrical Metasurfaces with Spatially-Varying Impedance Distribution *Radioengineering* **2019**, *28*, 505–511.
25. Li, J.; Diaz-Rubio, A.;Jia, Z.; Shen, C.; Tretyakov, S.; and Cummer, S. Highly Efficient Generation of Angular Momentum with Cylindrical Bianisotropic Metasurfaces *Phys. Rev. Appl.* **2019**, *11*, 024016.
26. Xu, G.; Eleftheriades, G. V.; and Hum, S.V. Discrete-Fourier-Transform-Based Framework for Analysis and Synthesis of Cylindrical Omega-Bianisotropic Metasurfaces *Phys. Rev. Appl.* **2020**, *14*, 064055.
27. Lin, C.W.; and Grbic, A., "Analysis and Synthesis of Cascaded Cylindrical Metasurfaces using a Wave Matrix Approach," *IEEE Trans. Antennas Propag.* early access
28. Asadchy, V.S.; Díaz-Rubio, A.; Tretyakov S.A. Bianisotropic metasurfaces: Physics and applications *Nanophotonics* **2018**, *7*, 1069–1094.
29. J. A. Kong, Theorems of bianisotropic media, Proc. IEEE, 60, 1036 (1972).
30. J. Vehmas, S. Hrabar, and S. Tretyakov, "Omega transmission lines with applications to effective medium models of metamaterials,"*Phys. Rev. Appl.* **2014**, *115*, 134905.
31. Yu, N.; Genevet, P.; Kats, M.A.; Aieta, F.; Tetienne, J.P.; Capasso, F.; and Gaburro, Z. Light Propagation with Phase Discontinuities: Generalized Laws of Reflection and Refraction *Science* **2011**, *334*, 333–337.
32. D.M. Pozar, *Microwave Engineering*, 4th ed. New York:Wiley, 2011 pp. 191–194.
33. Dorrah, A.H.; Chen. M.; Eleftheriades, G. V. Bianisotropic Huygens' Metasurface for Wideband Impedance Matching Between Two Dielectric Media *IEEE Trans. Antennas Propag.* **2018**, *66*, 4729–4742.
34. Pfeiffer, C.; Grbic, A. Metamaterial Huygens' Surfaces: Tailoring Wave Fronts with Reflectionless Sheets *Phys. Rev. Lett.* **2013** *110* 197401
35. Selvanayagam, M.; Eleftheriades, G.V. Discontinuous electromagnetic fields using orthogonal electric and magnetic currents for wavefront Manipulation *Optics Express***2013** *21, 12* 14409-14429
36. Epstein, A; Eleftheriades, G.V. Huygens' metasurfaces via the equivalence principle: design and applications *J. Opt. Soc. Am. B* **33**, A31-A50 (2016)
37. Achouri, K.; Salem M.A. and Caloz, C. General Metasurface Synthesis Based on Susceptibility Tensors *IEEE Trans. on Ant. and Prop.*, **63**, 7, 2977-2991, (2015)
38. Luukkonen O.; Simovski, C.; Granet, G.; Goussetis, G.; Lioubtchenko, D.; Räisänen, A.V.; Tretyakov, S. "Simple and Accurate Analytical Model of Planar Grids and High-Impedance Surfaces Comprising Metal Strips or Patches," *IEEE Transactions on Antennas and Propagation*, **2008** *56*, 1624-1632.
39. Langley, R.J.; and Parker, E. A. "Equivalent circuit model for arrays of square loops," *Electronics Letters*, **1982** *18*, 294–296.
40. J. P. S. Wong; A. Epstein and G. V. Eleftheriades Reflectionless Wide-Angle Refracting Metasurfaces *IEEE Antennas and Wireless Propagation Letters* **2016**, *15*, 1293–1296.
41. B. O. Raeker and A. Grbic Compound Metaoptics for Amplitude and Phase Control of Wave Fronts *Phys. Rev. Lett.* **2019**, *122*, 113901.
42. A. H. Dorrah and G.V. Eleftheriades Bianisotropic Huygens' Metasurface Pairs for Nonlocal Power-Conserving Wave Transformations, *IEEE Antennas Wirel. Propag. Lett.*, **2018**, *17* 1788–1792.

43. Popov, V.; Boust, F.; Tretyakov, S.; Burokur, S. N. Omega-bianisotropic metasurface for converting a propagating wave into a surface wave *Phys. Rev. B* **2019**, *100*, 125103.
44. Budhu, J; and Grbic, A., "Perfectly Reflecting Metasurface Reflectarrays: Mutual Coupling Modeling Between Unique Elements Through Homogenization," *IEEE Trans. Antennas Propag.* **2021**, *69*, 122–134.
45. Chiotellis, N.; and Grbic A., "Analytical modeling of tensor metasurfaces," *J. Opt. Soc. Am. B* **2021**, *33*, A51–A60.
46. Yang, F.; Raeker, B.O.; Nguyen D.T; Miller J.D.; Xiong, Z; Grbic, A.; Ho, J.S. “Antireflection and Wavefront Manipulation with Cascaded Metasurfaces,” *Phys. Rev. Applied*, **2020** *14*, 064044.